New Aspects of the α-Helix to β-Sheet Transition in Stretched Hard α-Keratin Fibers

L. Kreplak, J. Doucet, P. Dumas, and F. Briki
LURE (Laboratoire pour l'Utilisation du Rayonnement), Centre Universitaire Paris-Sud, 91898, Orsay cedex, France

ABSTRACT The putative transformation of α-helices into β-sheets has been studied for more than 50 years in the case of hard α-keratin. In a previous study of stretched keratin fibers, we specified the conditions for β-sheet appearance within horsehair: the formation of β-sheets requires at least 30% relative humidity. However, this phenomenon was observed in the whole tissue. Then there was no clear chemical identification of the β-sheets (keratin or matrix proteins) and the exact location of the β-sheets across the fiber could not be specified. In this study, using wide-angle x-ray scattering and high spatial resolution infrared microspectroscopy, we could determine and characterize the structural elements across hair sections stretched in water, which provides new information about the aforementioned transition. Our results show that the process can be split into three steps: 1), unraveling of the α-helical coiled-coil domains, which starts at roughly 5% macroscopic strain; 2), further transformation of the unraveled coiled-coils into β-sheet structures, which occurs above roughly 20% macroscopic strain; and 3), spatial expanding of the β-structured zones from the sample center to its periphery.

INTRODUCTION

During their production by the cell machinery or to perform their functions, proteins are subjected to large structural transitions. Such processes have been extensively analyzed in vitro (Fay et al., 2003; Krieger et al., 2003; Mok et al., 2003; Segel et al., 1999), but little is known about these phenomena in cells or tissues. More recently, the discovery of harsh human diseases related to the irreversible structural transition of α-helices to β-sheets (Stefani and Dobson, 2003; Zanusso et al., 2001) has given a new impetus to the study of the $\alpha \rightarrow \beta$ transition. This structural change was observed for the first time in stretched hard α-keratin fibers (human hair, porcupine quill, wool, etc.) (Astbury and Street, 1931; Astbury and Woods, 1933; Bendit, 1957).

Hard α-keratin fiber is a hierarchically structured material that shows a fibrous organization from the micrometer to the nanometer scale (Zahn et al., 1980). The main part of the fiber, called the cortex, is composed of spindle-shaped cells of $\sim$100 μm long and 3 μm wide. These cells contain macrofibrils of 0.3-μm diameter which are glued together by an intermacrofibrillar matrix. The macrofibril structure is also composite; it consists of a two-dimensional array of cylindrical shaped units of 7.5-nm diameter named the microfibrils. These units are embedded in a hydrophilic sulfur-rich protein matrix (Zahn et al., 1980). Like other intermediate filaments (IFs), the microfibrils, i.e., the hard α-keratin IFs, consist of a complex axial and radial assembly of heterodimers (Parry and Steinert, 1999). The main molecular feature of the $\sim$50-nm-long heterodimer consists of a central rod domain composed of a double stranded α-helical coiled-coil interrupted by nonhelical segments. Head and tail domains of unknown structure surround the central rod domain.

In the quiescent state, the fiber's well-defined molecular structure gives rise to the wide-angle x-ray diffraction (WAXS) pattern shown in Fig. 1 *a*. We can clearly distinguish two major reflections superimposed to a diffuse halo around 0.45 nm, which is characteristic of disordered amorphous polypeptide chains:

1. The sharp 0.52-nm meridian arc proceeds from the combination of the axial periodicity of roughly 47 nm along the microfibril with the regular geometry of the coiled-coil domains. This spacing is directly related to the α-helix pitch projection along the coiled-coil axis. This arc is superimposed to a broader one centered at around 0.5 nm, which probably arises from less ordered coiled coils (Busson et al., 1999a).
2. The broad equatorial spot at 0.96 nm corresponds to the mean distance between adjacent α-helical axes.

For samples stretched to 100% length in hot steam, the WAXS pattern is qualitatively different as shown in Fig. 1 *b*. Three major features can be seen, as already reported (Fraser et al., 1969):

1. The sharp 0.333-nm meridian arc arises from the distances between residues along the polypeptide chain in a regular β-sheet conformation.
2. The 0.465-nm equatorial arc arises from the lateral distances between chains in a β-sheet structure. This distance is imposed by main-chain hydrogen bond geometry.
3. The broad equatorial spot near 0.96 nm corresponds roughly to a mean intersheet distance.

Submitted November 3, 2003, and accepted for publication April 2, 2004.

Address reprint requests to Dr. Fatma Briki, Laboratoire LURE-Bât 209 D, Centre Universitaire Paris-Sud, 91898, Orsay cedex, France. E-mail: briki@lps.u-psud.fr.

L. Kreplak's present address is M. E. Müller Institute, Biozentrum, University of Basel, Klingelbergstrasse 70, 4056 Basel, Switzerland.

© 2004 by the Biophysical Society

0006-3495/04/07/640/08 $2.00

doi: 10.1529/biophysj.103.036749

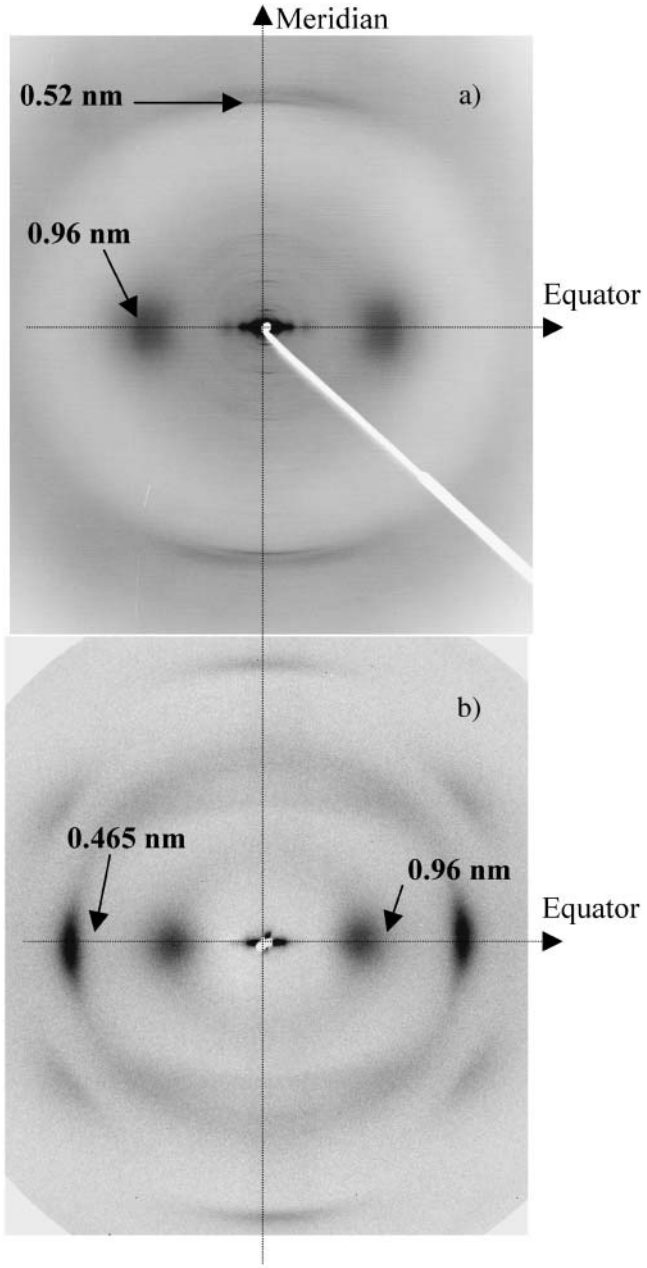

FIGURE 1 (*a*) Typical WAXS pattern of hard α-keratin from horsehair. The fine 0.52-nm arc is visible on the meridian axis above a broader arc around 0.5 nm, whereas the broad 0.96-nm maximum appears on the equator. Notice the weak and diffuse ring around 0.45 nm. (*b*) Typical WAXS pattern of β-keratin obtained from horsehair stretched to 100% extension in steam. The 0.333-nm arc is visible on the meridian, whereas the 0.465-nm arc appears on the equator together with a broad 0.96-nm maximum.

The presence of all these three features on a diffraction pattern is required to ensure the existence of $\beta-$sheets in the fiber.

The native and stretched keratin fibers have also different infrared spectra in the Amide I band region as shown in Fig. 2 for spectra taken in the cortex (Bendit, 1966). For the

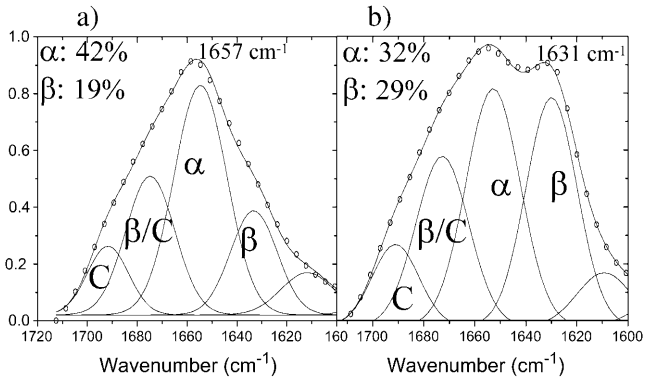

FIGURE 2 Typical infrared amide I band spectra taken in the cortex of a horsehair fiber at 0% strain (*a*) and stretched to 100% extension in steam (*b*). The fits have been done using four contributions: 1), a band centered around 1651–1657 cm^{-1} named α; 2), a band centered around 1621–1631 cm^{-1} named β; 3), a band centered around 1687–1692 cm^{-1} named C; and 4), a band centered around 1671–1685 cm^{-1} named β/C.

native fiber, the band is centered at 1657 cm^{-1}, which is the major frequency of the vibration spectrum of a polypeptide chain in the α-helix conformation (Stuart, 1997). For the stretched fiber, the Amide I band shows a second maximum at 1631 cm^{-1}, which is the major frequency of the vibration spectrum of a polypeptide chain in the β-sheet conformation (Stuart, 1997).

Encouraged by the textile industry, a great amount of work using essentially x-ray diffraction techniques (Bendit, 1960) and differential scanning calorimetry (Spei and Holzem, 1987) has been undertaken. This made it possible to develop models relating the structural transition of the coiled-coil domains to the macroscopic mechanical properties of keratin fibers (Bendit and Feughelman, 1968; Chapman, 1969; Hearle, 2000; Wortmann and Zahn, 1994). These models are based on the same molecular interpretation of the macroscopic tensile properties that was first proposed by Bendit using x-ray diffraction data (Bendit, 1960). That is:

1. The α-helix to β-sheet transition occurs above 5% macroscopic strain and under any humidity condition.
2. The microscopic extension of the polypeptide chains is equal to the applied macroscopic strain.
3. As a consequence of assumptions 1 and 2, the increase in β-sheet content varies linearly with the applied strain above 5% strain.

This model is now challenged by various studies (Cao, 2000; Kreplak et al., 2001; Fudge, 2003). Concerning assumption 1, we have demonstrated in a previous study that in horsehair stretched at 30% relative humidity, the coiled coils were only unraveled without transforming into β-sheets. We have also shown in the same study that the transformation occurs only above roughly 20% strain for wet fibers (Kreplak et al., 2001). One can also question about assumption 2, since it has been observed that the microscopic strain, as estimated from the displacement of the meridian

small-angle x-ray scattering reflection at 6.7 nm, was always smaller than the applied macroscopic strain (Kreplak et al., 2002).

The aforementioned studies clearly show the need of revisiting the $\alpha \rightarrow \beta$ transition mechanism in hair keratin. For this purpose, we have used WAXS and synchrotron radiation-based infrared microspectroscopy (Carr and Williams, 1997) to probe the relationship between macroscopic strain and the spatial distribution of the $\alpha \rightarrow \beta$ transition. We show that the $\alpha \rightarrow \beta$ transition occurs above 20% macroscopic strain. This transition is consistent with the unfolding of the α-helical coiled coils of keratin molecules below 20% strain followed by a folding into β-sheets. The simultaneous presence of α and β conformations up to ~50% strain is mainly due to the $\alpha \rightarrow \beta$ transition chronology; the transformation first occurs in the fiber core and then propagates to its periphery. This behavior indicates a strain gradient across the fiber section that is likely related to the crystalline grade of the keratin material.

MATERIALS AND METHODS

Samples

All the experiments were carried out on horsehair fibers taken from the tail. No special treatment was used except for a short cleaning in water. The samples were ~0.2 mm in diameter.

Mechanical setup

The stretching frame was composed of two jaws. One was fixed, whereas the other was set on a screw to stretch the fiber. The distance between the jaws prior to stretching was set to 14.5 mm. In the case of the WAXS experiments, a step-by-step stretching with a 1.7% macroscopic-strain step size was chosen. This procedure allowed us to follow accurately the behavior of the various scattering patterns as a function of the applied macroscopic strain. A WAXS pattern was recorded at each step. The strain was maintained constant during the exposures but a slight mechanical stress relaxation was observed.

For the infrared microspectroscopy experiments, it was possible to use a continuous stretching with a rate of 6.9% macroscopic strain per minute; this enabled us to ignore possible mechanical relaxation (Peters and Woods, 1956). In both cases, the samples were immersed in water at room temperature during stretching.

X-ray scattering experiments

X-ray scattering setup

Data collection was performed at the synchrotron x-ray source of LURE at Université Paris-Sud on a D43 beamline. We used a collimated and monochromatic incident beam of 0.5-mm section diameter. A transmission geometry setup was chosen with the samples mounted on the stretching frame oriented perpendicular to the incident beam. The wavelength was set to 0.145 nm and the sample-to-detector distance was 100 mm. Exposure time of 10 min was used for all the experiments.

Two-dimensional scattering patterns were recorded on Fuji imaging plates set perpendicular to the incident beam. The plates were read on a PhosphorImager 400E scanner (Molecular Dynamics, Sunnyvale, CA) with a pixel size of 0.176×0.176 mm^2. One-dimensional meridian and equatorial profiles passing through the origin have been extracted from the two-dimensional patterns by integrating the intensity around the meridian on a 12-pixel-thick rectangular strip.

Data treatment

Air scattering contribution and sample absorption were accounted for by calculating a corrected intensity for each pattern: $I_{\text{corrected}} = I_{\text{sample}} - I_{\text{air}}$, where I_{sample} and I_{air} are, respectively, the scattered intensities by the sample and the air normalized to the intensity of the transmitted beam measured with a photodiode. Since the beam diameter was larger than that of the fiber, an additional intensity correction was performed to normalize $I_{\text{corrected}}$ to the diameter of the sample that decreased during extension. However, to avoid separate measurements of hair diameter during stretching, we used as a scaling factor the value that allowed the intensity profiles to superimpose at wide diffraction angles.

Infrared microspectroscopy experiments

Sample preparation and control

To characterize the effect of the sample preparation procedure on the keratin structure, WAXS patterns were recorded for three groups of four horsehair fibers. From each group, fibers were stretched in water at constant speed to various macroscopic strains: 0, 20, 40, and 60%. The first group, named control 1, was used for WAXS measurement in air just after stretching, without relaxing the strain. The two other groups were put in hot steam at 100°C for 1 h at constant strain. After this treatment, one group, named control 2, was used for WAXS measurement in air. Exposure times of 10 min were used for recording all the diffraction patterns. The last group was prepared for infrared spectroscopy analysis. The samples from this group were embedded in a resin that was left polymerizing for 4 days at 60°C. Using a microtome, these samples were sliced to yield 3-μm-thick cross sections that were placed on ZnS slits for the infrared measurements.

Data collection

Infrared spectra were collected using a Spectra Tech (Shelton, CT) infrared microscope with a small aperture (11×11 μm^2) on beamline MIRAGE at SuperACO, LURE, France (Polack et al., 1999). After viewing the horsehair section with an optical microscope, the area to be sampled was set manually using two adjustable confocal apertures. The optical microscope was then switched to its infrared configuration, allowing the infrared beam to pass through the sample area determined by the apertures. An automated *x-y* mapping stage allowed the sample to be linearly or raster scanned, with a step accuracy of 1 μm. For the data reported here, infrared spectra were recorded with a resolution of 8 cm^{-1}, and either 128 or 256 scans were coadded before Fourier transform processing.

Data treatment

After linear baseline subtraction, to account for the gradual decay of the synchrotron beam intensity, two kinds of treatments were performed. Absorption intensity maps were constructed from the spectra at each pixel, either using heights of selected peaks or integrated areas. Moreover, the amide I band (1600–1700 cm^{-1}) of each spectrum was subjected to a fitting procedure using five Gaussian distributions (25 cm^{-1} full width at half maximum) centered at the frequencies of well-characterized secondary structures (Stuart, 1997). During the fitting procedure the peak heights were not constrained, whereas peak positions were constrained within a limited interval. The fitting procedure was achieved using the fitting ''module'' of the Origin package. It is worthwhile to note that all the frequencies were present on the second derivative of the spectra. Integrating the area of each peak and then normalizing it to the total area of the amide I band assessed the contribution of each peak to the amide I band.

RESULTS

Modification of the WAXS pattern during stretching

The intensity behaviors of the meridian zone around 0.5 nm, the 0.95-nm equatorial spot, and the 0.465-nm equatorial arc were analyzed as a function of the applied macroscopic strain. Along the meridian, attention was mainly focused on the intensity behavior of the broad arc centered near 0.5 nm at 0% strain. That was the only one remaining above 5% macroscopic strain. Selected profiles extracted in this zone for several strain values are shown in Fig. 3 *a*. The arc intensity, as estimated from its height at the position $S = 1/5.2\ \text{nm}^{-1}$, decreases linearly with the macroscopic strain above 5–10%. This is shown in the inset of Fig. 3 *a*. Just before fiber failure at 53% macroscopic strain the initial broad arc is simply transformed into a small hump above the amorphous halo and a diffuse peak appears around 0.33 nm. Note that the experimental setup was not chosen to focus on this particular zone of the reciprocal space (see Kreplak et al., 2001).

The behavior of the equatorial features is shown in Fig. 3 *b*. The position of the 0.95-nm spot is nearly independent of the strain. Its intensity decreases similarly to that of the 0.5-nm meridian arc. The 0.465-nm arc appears only between 20 and 25% macroscopic strain (Fig. 3 *b*). Its intensity increases linearly with strain as shown in the Fig. 3 *b* inset.

Modification of the WAXS pattern during the sample preparation for the infrared microspectroscopy experiments

In a first stage, the samples were stretched at 6.9% strain per minute in water. The corresponding patterns are shown in Fig. 4 (control 1). The strong small-angle scattering is due to a bad positioning of the beam stop. At 20% strain, the pattern is close to that of nonstretched samples (Fig. 1 *a*); only the sharp 0.52-nm meridian arc disappeared. The strong 0.5-nm meridian arc remains unchanged. At 40% and 60% strain the broad 0.5-nm meridian arc becomes more diffuse and the 0.465-nm arc along the equator appears clearly. These results are consistent with the behavior obtained for the step-by-step stretching experiment.

In a second stage, the samples were exposed to hot steam at constant length after stretching in water at constant speed. The corresponding patterns are shown in Fig. 4 (control 2). At 20% strain the pattern is similar to the one of a nonstretched sample (Fig. 1 *a*), except for the presence of a weak 0.465-nm equatorial arc. At strain 40 and 60%, the patterns are similar to those obtained for samples stretched at 100% in hot steam (Fig. 1 *b*), with all the features characteristic of well-defined β-sheet structures. No significant changes could be detected in WAXS patterns of these same samples 15 days after the first measurements. It is also worth noting that the x-ray scattering pattern of the nonstretched sample is not modified by hot steam treatment at constant length.

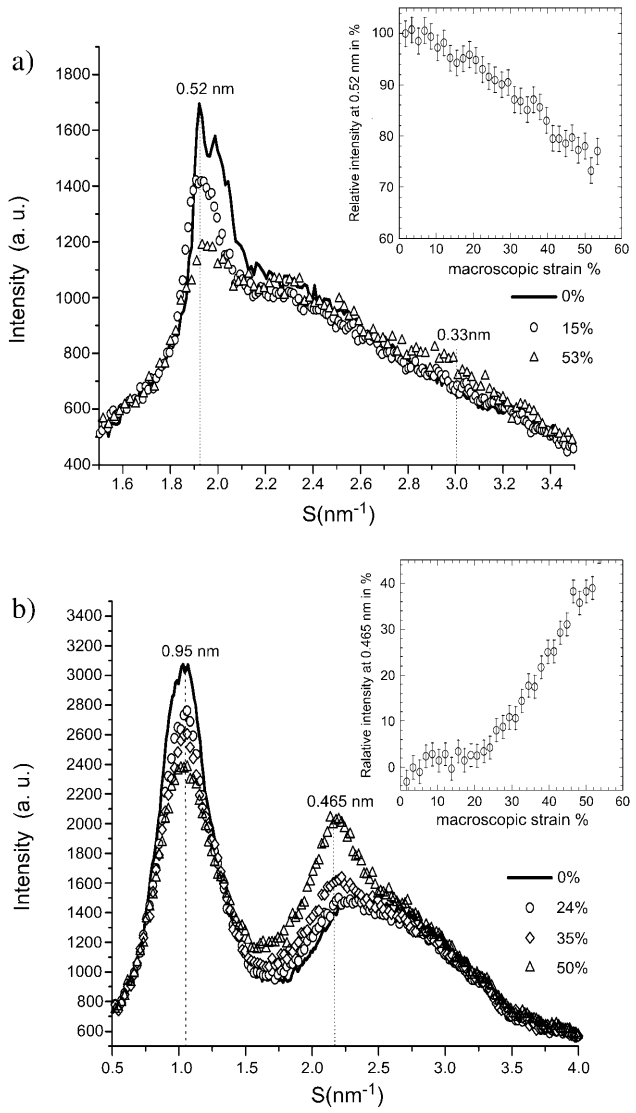

FIGURE 3 (*a*) One-dimensional profiles extracted along the meridian at 0, 15, and 53% macroscopic strain corresponding to the step-by-step experiment. *Inset*: Relative intensity at $S = 1/0.52\ \text{nm}^{-1}$ versus macroscopic strain. The contribution of the amorphous halo around 0.45 nm to this intensity is roughly constant upon stretching and can be approximated to 900 au. (*b*) One-dimensional profiles extracted along the equator at 0, 24, 35, and 50% macroscopic strain corresponding to the step-by-step experiment. *Inset*: Relative intensity at 0.465 nm versus macroscopic strain. Notice the linear increase above 20% strain.

Infrared microspectroscopy data

Using the infrared spectra collected across the sections of the samples stretched at 0, 20, 40, and 60%, maps of the band intensity at 1631 cm^{-1} were constructed (Fig. 5 *a*). The green regions have amide I band massifs similar to the one in Fig. 2 *a*, with a single maximum at 1657 cm^{-1}. The regions

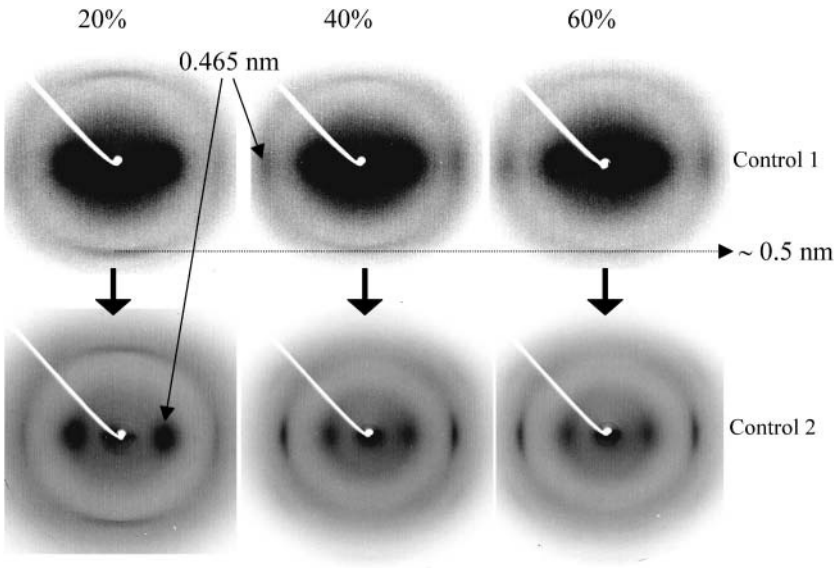

FIGURE 4 Gallery of WAXS patterns taken for horsehair fibers stretched continuously in water to 20, 40, and 60% strain (control 1) and then exposed to steam for 1 h at constant length (control 2).

colored in red have amide I band massifs similar to the one in Fig. 2 *b* with two well-defined maximums at 1631 and 1657 cm^{-1}. Note that the map for the sample at 60% strain is not presented in Fig. 5 *a* because of its similarity to the one obtained for the 40% strain sample.

At 0% strain, the map is clearly homogeneous with a high α-helical content as confirmed by the WAXS pattern of the sample. At 40% strain, the map is also homogeneous and indicates the presence of a large amount of β-sheets; this result is consistent with the corresponding WAXS pattern presented in Fig. 4 (control 2). At 20% strain the sample is clearly biphasic, with an α-helix-rich outer layer and an inner core containing β-sheets. The infrared map is consistent with the corresponding WAXS pattern reported in Fig. 4 (control 2).

To clearly characterize the biphasic nature of the 20% strain sample, we have extracted spectra along a 160-μm-long line shown in Fig. 5 *a*. The amide I band massifs of the different spectra have been plotted in Fig. 5 *b*; the variations of the intensities at 1631 and 1657 cm^{-1} are opposite. Each massif has been fitted according to the procedure described above. The contribution of each band to the total massif area is plotted as a function of the position along the line (Fig. 5, *c–d*). The bands at 1631 and 1657 cm^{-1}, named β and α, respectively, display opposite behaviors. The first band presents a maximum centered near 80 μm and the second one a minimum at the same position (Fig. 5 *c*). The two other bands (named C and β/C, respectively) are nearly independent on the position along the line (Fig. 5 *f*).

DISCUSSION

From the combination of WAXS and infrared microspectroscopy measurements on stretched wet horsehair fibers, we propose an updated keratin α-helix to β-sheet transformation mechanism which is different from the existing one proposed by Bendit (1960).

The $\alpha \rightarrow \beta$ transformation consists of a two-stage mechanism

One of the main aspects of the $\alpha \rightarrow \beta$ transformation mechanism proposed by Bendit is the linear relationship between the applied macroscopic strain and the amount of the β-sheet formation (see Fig. 5 in Bendit, 1960). Our observations are clearly in disagreement with such a mechanism. The x-ray scattering profiles of Fig. 3 and the two-dimensional patterns of Fig. 4 ''control 1'' indicate that β-sheet structures only appear above 20–25% macroscopic strain, whereas the $\alpha-$helix fiber content decreases in the first few percentages of strain. The discrepancy is probably related to Bendit's interpretation; there was no distinction made between the unraveling stage and the refolding stage. It is worth mentioning that in earlier works of Peters and Woods, in 1956, it was noticed that the formation of the β-sheet structures required at least 20% strain. This is in agreement with our measurements. Unfortunately these authors did not report the intensity decrease of the 0.5-nm meridian arc above 5% strain. This decrease is important since it reveals a progressive unraveling of the coiled-coil domains, similar to the main molecular deformation pathway observed for fibers stretched at 30% relative humidity (Kreplak et al., 2001). However, this intermediate unraveling process would not be compatible with our data if we assume a uniform occurrence across the whole fiber. The coexistence of α and β scattering features at 20% and 40% strain could indeed indicate that the coiled coils unraveling and the β-sheet formation are unrelated. This coexistence has already been reported in the case of fibers stretched in water below 20% and then steamed (Feughelman, 1960). Since the

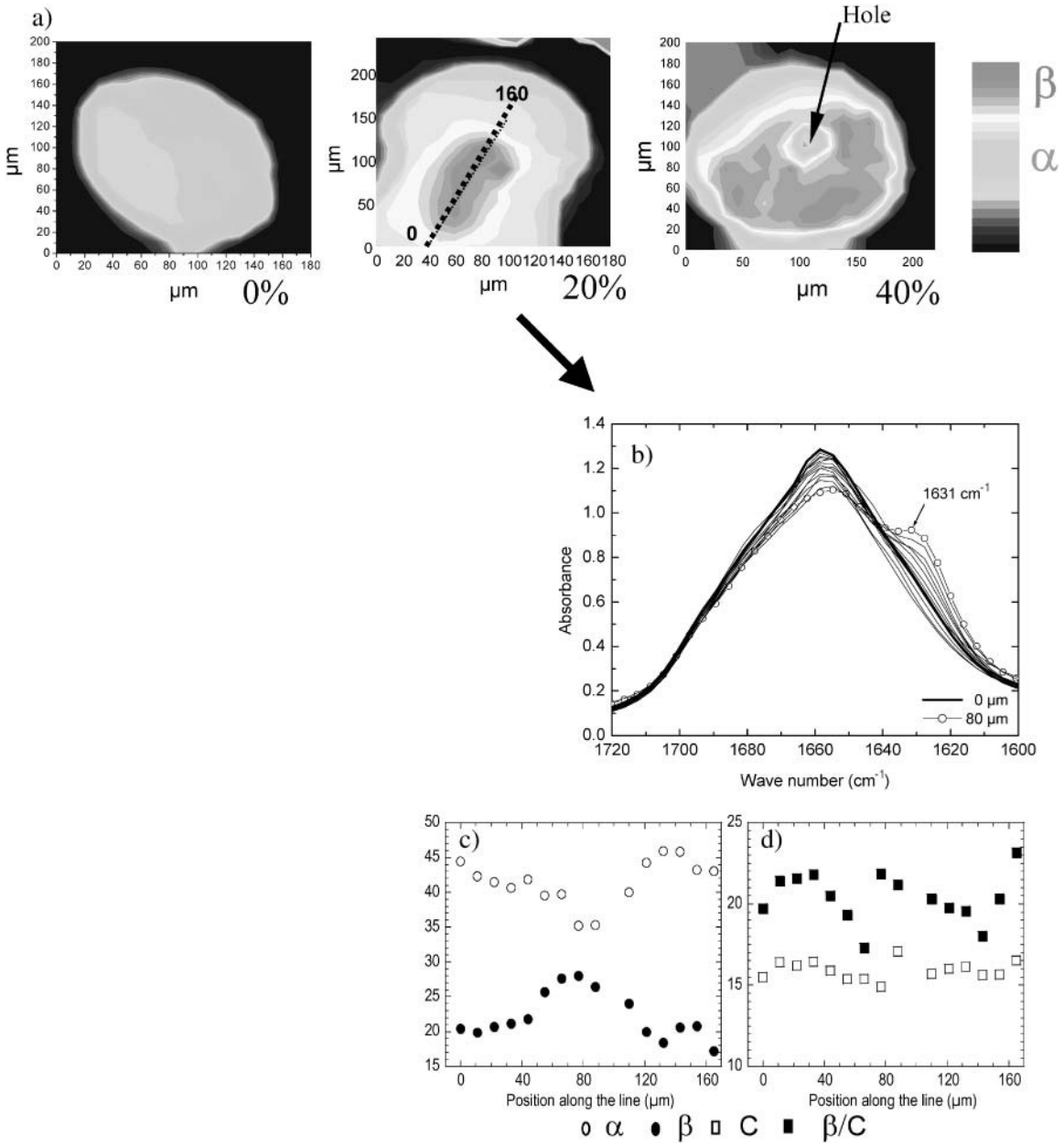

FIGURE 5 (*a*) Absorption maps at 1631 cm^{-1} obtained after processing of infrared spectra taken across horsehair sections stretched continuously in water to 20, 40, and 60% strain and then exposed to steam for 1 h at constant length. In light shaded is the region rich in α-helices where the amide I band is similar to the one in Fig. 2 *a*. In dark shaded is the region containing β-sheets where the amide I band is similar to the one in Fig. 2 *b*. (*b*) Amide I band spectra extracted along the dotted line highlighted in the 20% strain sample absorption map. These spectra have been fitted using the four bands described in Fig. 2, *c* and *d*. Evolution of the proportion of the four fitted bands as a function of the position along the dotted line.

pioneer work of Astbury, steam is known to set the structure of stretched fibers (Feughelman, 1968). Our infrared maps of steamed hair sections allow us to conclude that the coexistence of α and β structures is due to a nonuniform process across the section; the β-sheets first appear in the fiber core and gradually extend to the whole fiber while stretching. Consequently, our x-ray scattering data are consistent with a two-stage mechanism involving the unraveling of coiled-coil domains to stretched disordered chains before the β-sheet structure formation, as already suggested by Skertchly and Woods (Skertchly and Woods, 1960).

The β-sheet structures arise from a coiled-coil unfolding-refolding process

β-sheet structures could either arise from a refolding of the unraveled keratin α-helices or from other nonkeratinous

proteins, which did not give rise to any diffraction signal before stretching and would transform into β-sheets under stretching. Our results strongly support the hypothesis of a refolding of the unraveled keratin molecules. The first argument is given by the intensity of the scattering features. The intensity arising from β-sheets in the stretched sample is comparable to the intensity arising from α-helices in the nonstretched one, which is indicative of similar concentrations of α-helices and β-sheets. The only component that could give the same scattering contribution is the intermicrofibrillar matrix, which is known to contain various sulfur-rich proteins (Fraser at al., 1972). However, it is unlikely that all these globular small proteins could transform into β-sheets following the same kinetics as the coiled-coil unfolding. A second indication is given by the secondary structure signals observed across the infrared hair section maps at 20% strain. The distributions of the signals along lines passing through the axis are given in Fig. 5, *C–D*. The α and β bands are clearly anticorrelated, whereas the coil and β/coil bands remain nearly constant along the line.

It is therefore highly probable that the $\alpha \rightarrow \beta$ transition is due to an unfolding-refolding process of the IF keratin molecules. This conclusion confirms recent results on hagfish slime thread stretching (Fudge et al., 2002). This tissue, which consists of almost pure keratin-like IFs, exhibited an $\alpha \rightarrow \beta$ transition that can only arise from the conformational change of IFs' composing heterodimers.

The amount of $\alpha \rightarrow \beta$ transformation is linked to the fiber crystalline grade

The coexistence of α and β structures across the fiber section stretched at 20% and 40% strain may seem surprising. The propagation of $\alpha \rightarrow \beta$ transition from the core to the periphery during stretching is probably due to a radial microscopic stress gradient. The local stress would depend on the distance to the hair axis, the highest stress being located along the fiber axis. Such behavior, not expected for a uniform sample, is clearly due to a nonuniform macroscopic structure. A gradient of keratin crystalline quality across the hair section has already been revealed by microdiffraction studies of human and horsehair (Busson et al., 1999b). The cortex core showed a more ordered architecture than the outer cortex zone; a stress gradient may arise from this structural gradient.

In a previous study, we showed that two processes are in competition at the molecular scale during hair-fiber stretching in water: a stretching of the coiled coils and a sliding of the molecules along each other (Kreplak et al., 2002). In well-crystallized zones, as in the core, the stretching process should prevail over the sliding one and therefore would favor the unfolding-refolding transformation into β-sheets. On the contrary, in poorly crystallized zones, the sliding process would prevail up to $\sim$30% strain (Kreplak et al., 2002) without affecting significantly the molecular structure. The consequence of the two processes would result in a biphasic sample at 20% strain, with a β-sheet-rich core and an α-helical-rich periphery. Further strain increase would lead finally to a complete transformation into β-sheets over the whole cross section. Let us note that our observation of the transverse α/β gradient is complementary but not contradictory to the more rapid appearance of β-sheets in stretching-induced necked zones than in unnecked zones along the fiber (Cao at al, 2002).

In summary, WAXS and infrared microspectroscopy experiments on stretched wet horsehair fibers allowed us to get a new insight into the $\alpha \rightarrow \beta$ transition mechanism in keratinous fibers. We show that the structural transition in wet hair keratin under stretching is a two-stage process where the α-helices are unraveled without any molecular ordering before transforming into β-sheets. Moreover, we reveal and follow, for the first time, the spatial expanding of the $\alpha \rightarrow \beta$ transition during stretching; this propagates from the sample center to its periphery. This expanding is most likely related to the crystalline quality. Further information from this study concerns the role played by water, which seems to act as a polymer plasticizer in the transformation mechanism: stretching in water leads to the formation of β-sheets, whereas the chains remain unraveled at low-humidity conditions.

Using these new data, one has to revisit the molecular interpretations of the various mechanical and thermal properties of hard α-keratin fibers.

REFERENCES

Astbury, W. T., and A. Street. 1931. X-ray studies of the structure of hair, wool and related fibers. I. *General. Trans. Roy. Soc.* 230A:75–101.

Astbury, W. T., and H. J. Woods. 1933. X ray studies of the structure of hair, wool, and related fibres. II. The molecular structure and elastic properties of hair keratin. *Phil. Trans. R. Soc. Lond.* A. 232:333–394.

Bendit, E. G. 1957. The alpha-beta transformation in keratin. *Nature.* 179:535.

Bendit, E. G. 1960. A quantitative x-ray diffraction study of the alpha-beta transformation in wool keratin. *Text. Res. J.* 30:547–555.

Bendit, E.G. 1966. Infrared absorption spectrum of keratin. I. Spectra of alpha-, beta-, and supercontracted keratin. *Biopolymers.* 4:539–559.

Bendit, E. G., and M. Feughelman. 1968. Keratin. *Encyclopedia of Polymer Science.* 8:1–44.

Busson, B., F. Briki, and J. Doucet. 1999a. Side-chains configurations in coiled coils revealed by the 5.15-A meridional reflection on hard alpha-keratin X-ray diffraction patterns. *J. Struct. Biol.* 125:1–10.

Busson, B., P. Engström, and J. Doucet. 1999b. Existence of various structural zones in keratinous tissues revealed by X-ray microdiffraction. *J. Synchrotron Rad.* 6:1021–1030.

Cao, J. 2002. Is the alpha-beta transition of keratin a transition of alpha-helices to beta-pleated sheets? Part II. Synchrotron investigation for stretched single specimens. *J. Mol. Struct.* 607:69–75.

Carr, G. L., and G. P. Williams. 1997. Infrared microspectroscopy with synchrotron radiation. *Proceedings of the SPIE.* 3153:51–58.

Chapman, B. M. 1969. A mechanical model for wool and other keratin fibers. *Text. Res. J.* 39:1102–1109.

Fay, N., Y. Inoue, L. Bousset, H. Taguchi, and R. Melki. 2003. Assembly of the yeast prion Ure2p into protein fibrils. Thermodynamic and kinetic characterization. *J. Biol. Chem.* 278:30199–30205.

Feughelman, M. 1960. The mechanical properties of set wool fibers and the structure of keratin. *J. Textile Inst.* 51:589–602.

Feughelman, M. 1968. The equilibrium between α and β phases in keratin fibers in water. *Text. Res. J.* 38:1136–1137.

Fraser, R. D. B., T. P. MacRae, D. A. D. Parry, and E. Suzuki. 1969. The structure of beta-keratin. *Polymer.* 10:810–826.

Fraser, R. D. B., T. P. MacRae, and G. E. Rogers. 1972. Keratins: Their Composition, Structure and Biosynthesis. Thomas, Springfield, IL. Chapters 2 and 3.

Fudge, D. S., K. H. Gardner, V. T. Forsyth, C. Riekel, and J. M. Gosline. 2003. The mechanical properties of hydrated intermediate filaments: insights from hagfish slime threads. *Biophys. J.* 85:2015–2027.

Hearle, J. W. 2000. A critical review of the structural mechanics of wool and hair fibers. *Int. J. Biol. Macromol.* 27:123–138.

Kreplak, L., J. Doucet, and F. Briki. 2001. Unraveling double stranded alpha-helical coiled-coils: an X-ray diffraction study on hard alpha-keratin fibers. *Biopolymers.* 58:526–533.

Kreplak, L., A. Franbourg, F. Briki, F. Leroy, D. Dalle, and J. Doucet. 2002. A new deformation model of hard alpha-keratin fibers at the nanometer scale: implications for hard alpha-keratin intermediate filament mechanical properties. *Biophys. J.* 82:2265–2274.

Krieger, F., B. Fierz, O. Bieri, M. Drewello, and T. Kiefhaber. 2003. Dynamics of unfolded polypeptide chains as model for the earliest steps in protein folding. *J. Mol. Biol.* 332:265–274.

Mok, K. H., T. Nagashima, I. J. Day, J. A. Jones, C. J. Jones, C. M. Dobson, and P. J. Hore. 2003. Rapid Sample-Mixing Technique for Transient NMR and Photo-CIDNP Spectroscopy: Applications to Real-Time Protein Folding. *J. Am. Chem. Soc.* 125:12484–12492.

Parry, D. A. D., and P. M. Steinert. 1999. Intermediate filaments: molecular architecture, assembly, dynamics and polymorphism. *Q. Rev. Biophys.* 32:99–187.

Peters, L., and H. J. Woods. 1956. Protein fibers. *In* R. Meredith, editor. Mechanical Properties of Textile Fibers. North-Holland Publishing, Amsterdam.

Polack, F., R. Mercier, L. Nahon, C. Armellin, J. P. Marx, M. Tanguy, M. E. Couprie, and P. Dumas. 1999. Optical design and performances of the IR microscope beamline at superACO. *Proc. SPIE.* 3775:13–21.

Segel, D. J., A. Bachmann, J. Hofrichter, K. O. Hodgson, S. Doniach, and T. Kiefhaber. 1999. Characterization of transient intermediates in lysozyme folding with time-resolved small-angle X-ray scattering. *J. Mol. Biol.* 288:489–499.

Skertchly, A. R. B., and H. J. Woods. 1960. The $\alpha \rightarrow \beta$ transformation in keratin. *J. Text. Inst.* 51:517–527.

Spei, M., and R. Holzem. 1987. Thermoanalytical investigations of extended and annealed keratins. *Coll. Polym. Sci.* 265:965–970.

Stefani, M., and C. M. Dobson. 2003. Protein aggregation and aggregate toxicity: new insights into protein folding, misfolding diseases and biological evolution. *J. Mol. Med.* In press.

Stuart, B., and D. J. Ando. 1997. Biological Applications of Infrared Spectroscopy. John Wiley & Sons, New York.

Wortmann, F. J., and H. Zahn. 1994. The stress/strain curve of alpha-keratin fibers and the structure of the intermediate filament. *Text. Res. J.* 64:737–743.

Zahn, H., J. Föhles, M. Nienhaus, A. Schwan, and M. Spei. 1980. Wool as a biological composite structure. *Ind. Eng. Chem. Prod. Res. Dev.* 19:496–501.

Zanusso, G., A. Farinazzo, M. Fiorini, M. Gelati, A. Castagna, P. G. Righetti, N. Rizzuto, and S. Monaco. 2001. pH-Dependent prion protein conformation in classical Creutzfeldt-Jakob disease. *J. Biol. Chem.* 276:40377–40380.